

Calculations of the Exciton Coupling Elements Between the DNA Bases Using the Transition Density Cube Method

Arkadiusz Czader and Eric R. Bittner*

Department of Chemistry, University of Houston, Houston TX 77204

(Dated: November 10, 2018)

Excited states of the of the double-stranded DNA model $(A)_{12} \cdot (T)_{12}$ were calculated in the framework of the exciton theory. The off-diagonal elements of the exciton matrix were calculated using the transition densities and ideal dipole approximation associated with the lowest energy $\pi\pi^*$ excitations of the individual nucleobases obtained from TDDFT calculations. The values of the coupling calculated with the transition density cubes (TDC) and ideal-dipole approximation (IDA) methods were found significantly different for the small inter-chromophore distances. It was shown that the IDA overestimates the coupling significantly. The effects of the structural fluctuations were incorporated by averaging the properties of the excited states over a large number of conformations obtained from the MD simulations.

I. INTRODUCTION

DNA a remarkable carrier of code of life, is very stable with respect to the photochemical decay. The path chosen by Nature to protect DNA is through the very rapid decay pathways of the electronic excitation energy. Given the importance of DNA in biological systems and its emerging role as a scaffold and conduit for electronic transport in molecular electronic devices, [1] DNA in its many forms is a well studied and well characterized system. What remains poorly understood, however, is the role that base-pairing and base-stacking plays in the transport and migration of the initial excitation along the double helix.[2, 3, 4]

The absorption of UV radiation by DNA initiate a number of photochemical reactions that can ultimately lead to carcinogenic mutations. [5, 6, 7, 8, 9] The UV absorption spectrum of DNA largely represents the weighted sum of the absorption spectra of its constituent bases. However, the distribution of the primary photochemical products of UV radiation, including bipyrimidine dimers, [10] is depends quite strongly upon base sequence, which implies some degree of coupling between the DNA bases. [3] Inasmuch as both the base stacking and base pairing are suspected to mediate the excess of electronic excitation energy, understanding of the excited-state dynamics is of primary importance for determining how the local environment affects the formation of DNA photolesions.

Recent work by various groups has underscored the different roles that base-stacking and base-pairing play in mediating the fate of an electronic excitation in DNA. [2, 3] Over 40 years ago, Löwdin discussed proton tunneling between bases as a excited state deactivation mechanism in DNA[11] and evidence of this was recently reported by Schultz *et al.* [12] In contrast, ultrafast fluorescence of double helix poly(dA)·poly(dT) oligomers

by Crespo-Hernandez *et al.*[2] and by Markovitsi *et al.* [3] give compelling evidence that base-stacking rather than base-pairing largely determines the fate of an excited state in DNA chains composed of adenosine and thymine bases with long-lived intrastrand states forming when ever adenosine is stacked with itself or with thymine. However, there is considerable debate regarding whether or not the dynamics can be explained via purely Frenkel exciton models [4, 13, 14] or whether charge-transfer states play an intermediate role. [15]

Upon UV excitation, the majority of excited molecules shows a subpicosecond singlet lifetimes. [16, 17, 18, 19] Owing to the technical difficulties in measuring the ultrashort lifetimes the study of the charge and excitation energy transfer in DNA has only recently received much of attention with the advances in the femtosecond spectroscopy. Although, so far, no clear picture of the excited-state deactivation mechanism has been offered by the experiment, two possible decay channels have been investigated. Kohler and coworkers in their recent study of the duplex poly(dA)·poly(dT) suggested that π -stacking of the DNA base determines the fate of a singlet electronic excited state.[2] Alternative decay mechanism involves interstrand hydrogen or proton transfer. Douhal and coworkers observed excited-state proton transfer in base pair mimics in gas-phase. [20] The experimental results suggests that these very fast decay pathways play an important role in quenching the reactive decay channels and providing DNA with intrinsic photochemical stability. However, they do not provide a clear picture which arrangement of bases, pairing or stacking, is of primary importance.

Until recently, most theoretical investigations of excitation energy transfer in DNA helices has been within the Frenkel exciton model which treats the excitation as a coherent hopping process between adjacent bases.[21, 22] This model has tremendous appeal since it allows one to construct the global excited states (i.e of the complete chain) in terms of linear combinations of local excited states. The key parameter in the evaluation of the electronic excitation energy transfer (EET) is the electronic coupling between the individual bases. To a first-

*John S. Guggenheim Fellow (2007)

order approximation, the base to base coupling can be estimated using a dipole-dipole approximation in which the interaction between the donor and acceptor is calculated using only the transition dipole associated with each chromophore. While this approach is certainly suitable for cases in which the distance between the donor and acceptor sites is substantially greater than the molecular length scale. In case of double stranded DNA, where the DNA bases are in relatively close contact compared to their dimensions this approach leads to the neglect of the effect of the size and spatial extent of the interacting transition densities associated with each chromophore.

By far the most precise way to calculate the coupling elements is to directly integrate the Coulomb coupling matrix element between transition densities localized on the respective basis.[23] The accuracy is then limited only by the numerical quadrature in integrating the matrix element and by the level and accuracy of the quantum chemical approach used to construct the transition densities in the first place. Furthermore, one must perform a quantum chemical evaluation of the coupling elements between each base at each snapshot along a molecular dynamics simulation in order to properly take into account the fluctuations and gyrations of the chain itself. This is a formidable task, one that has prevented an accurate benchmarking of the excited state electronic structure of realistic DNA chains.

In this paper, we present the results of simulations and calculations of accurate interbase exciton couplings for A-T strands of DNA in water in an attempt to provide such a benchmark. Starting from a molecular dynamics simulation of a model DNA sequence in water at the correct salt concentrations, we mapped out the evolution of the photochemically relevant excited states within a Frenkel exciton model in which the couplings were computed using both the ideal dipole-dipole approximation (IDA) and using the transition density cube approach (TDC).[23]

II. METHODOLOGY

The calculation procedure consisted of several steps. In the first stage the molecular dynamics (MD) calculations were carried out to sample a range of conformations of $(A)_{12} \cdot (T)_{12}$ model of DNA double-helix. The transition densities of the individual nucleobases obtained from time dependent density functional theory (TDDFT) calculations were subsequently superimposed with the instantaneous conformations from the MD simulations in order to calculate the coupling between the electronic transitions of the individual bases. In the final step, the excited-states of the model were calculated within the Frankel exciton model.

A. Exciton model

The excited states of the $(A)_{12} \cdot (T)_{12}$ were calculated in the framework of the exciton theory[24, 25]. In this approach the total Hamiltonian for the super system of N molecules is written as the sum of N Hamiltonians of isolated molecules H_n and the intermolecular interaction potential V_{nm} between the molecules n and m .

$$H = \sum_{n=1}^N H_n + \sum_{n=1}^N \sum_{m>n}^N V_{nm} \quad (1)$$

The singly excited states of the system are described in term of N locally excited configurations

$$\Phi_l^i = \phi_l^i \prod_{n \neq l} \phi_n \quad (2)$$

where ϕ_l^i corresponds to the excited state wavefunction of the chromophore l whereas all the other molecules m are in their ground state ϕ_n . Φ_l^i denotes the corresponding wave function of the super system. Consequently, the exciton states of the supramolecular system can be written as a linear combinations of the excited states localized on each chromophore.

$$\Phi_k = \sum_l c_{kl} |\Phi_l^i\rangle \quad (3)$$

The *diagonal elements* of the exciton matrix $\langle \Phi_n^i | H | \Phi_n^i \rangle$ are simply excitation energies of chromophore n from its ground to i^{th} excited state, $S_0 \rightarrow S_i$. The *off-diagonal elements* $\langle \Phi_n^i | H | \Phi_m^j \rangle$ written as $\langle \phi_n^i \phi_m^0 | V | \phi_n^0 \phi_m^j \rangle$ correspond to exciton coupling. It can be interpreted as the electrostatic interaction energy between the transition densities corresponding to $S_0 \rightarrow S_i$ and $S_0 \rightarrow S_j$.

A measure of delocalization of the exciton states can be obtained from the inverse participation ratio (IPR) ($1/L_k$) which represents the number of coherently coupled chromophores in a given eigenstate k . In the general case with more than one electronic transition per chromophore, L_k is written as follows:

$$L_k = \sum_{\text{molecules } m} \left[\sum_{\text{states } i} (C_{k,m}^i)^2 \right]^2 \quad (4)$$

where k denotes a given eigenstate and i an electronic excited state of a chromophore.

For purposes of developing a model, we can cast the exciton Hamiltonian as a $SU(2) \otimes SU(2)$ lattice model [26] consisting of localized hopping interactions for excitons between adjacent base pairs along each strand (t_{aj}) as well as cross-strand terms linking paired bases (h_i) and “diagonal” terms which account for the π stacking interaction between base j on one chain and base $j \pm 1$ on the other chain (r_i^\pm) in which r_j^- denotes coupling in the 5'-5' direction and r_j^+ coupling in the 3'-3' direction. Fig.

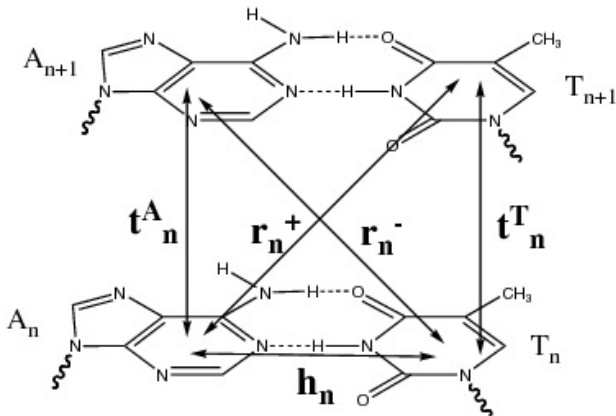


FIG. 1: Schematic view of the exciton coupling terms for Eq. 5.

1 shows a schematic view of the various coupling terms between each nucleotide base.

$$H = \sum_j \epsilon_j \hat{\psi}_j^\dagger \hat{\psi}_j + t_j (\hat{\psi}_{j+1}^\dagger \hat{\psi}_j + \hat{\psi}_j^\dagger \hat{\psi}_{j+1}) + h_j \bar{\psi}_j \hat{\psi}_j + \hat{\psi}_{j+1}^\dagger (r_j^+ \hat{\gamma}_+ + r_j^- \hat{\gamma}_-) \hat{\psi}_j + \hat{\psi}_j^\dagger (r_j^+ \hat{\gamma}_+ + r_j^- \hat{\gamma}_-) \hat{\psi}_{j+1}, \quad (5)$$

where $\hat{\psi}_j^\dagger$ and $\hat{\psi}_j$ are $SU(2)$ spinors that act on the ground-state to create and annihilate excitations on the j th adenosine or thymidine base along the chain. The $\hat{\gamma}$ operators are the 2×2 Pauli spin matrices with $\bar{\psi}_j = \hat{\gamma}_1 \hat{\psi}_j^\dagger$ and $\hat{\gamma}_+ + \hat{\gamma}_- = \hat{\gamma}_1$ providing the mixing between the two chains.

Taking the chain to homogeneous and infinite in extent, one can easily determine the energy spectrum of the valence and conduction bands by diagonalizing

$$\hat{H}(q) = \begin{pmatrix} \epsilon_A + 2t_A \cos(q) & h + r^+ e^{-iq} + r^- e^{+iq} \\ h + r^+ e^{+iq} + r^- e^{-iq} & \epsilon_T + 2t_T \cos(q) \end{pmatrix} \quad (6)$$

where $\epsilon_{A,B}$ and $t_{A,T}$ are local excitation energies and intra-strand hopping integrals. h is the coupling between Watson-Crick bases. When the interchain diagonal couplings are equal, $r^+ = r^-$, Eq. 6 is identical to the Hamiltonian used by Creutz and Horvath [27] to describe chiral symmetry in quantum chromodynamics in which the terms proportional to r are introduced to make the “doubblers” at $q \propto \pi$ heavier than the states at $q \propto 0$ since the off-diagonal coupling is now momentum dependent.

One of the *serious* deficiencies with this model as it stands thus far is that for DNA each of the interactions described is very sensitive to the geometric fluctuations of the DNA chain itself. [13, 14] Hence, we need to consider each of the couplings as being parametrically dependent upon the instantaneous molecular geometry of both the individual bases and the chain itself. This is assuming there is no additional contribution from the solvent and ions surrounding the DNA chain. Assuming that

the electronic time scale is fast compared to the typical time scale for geometric fluctuations of the DNA chain ($10^{-14} - 10^{-13}$ s for longitudinal and $10^{-13} - 10^{-12}$ s for the lateral motions of bases in DNA double helices[28]), we can consider at least the initial electronic dynamics as occurring in a fixed nuclear framework and subsequent dynamics as adiabatically following the nuclear motion. Nonadiabatic contributions can not be completely discounted; however, the dominant non-adiabatic couplings are intermolecular in origin or involve proton between adjacent bases. [11, 29, 30]

B. Transition densities and interactions

1. Exciton-exciton interactions

Each off-diagonal term in our Hamiltonian of Eq. 5 can be calculated according to

$$V^{Coul} = \sum_{ab} \frac{M_n^{0i}(a) M_m^{0j}(b)}{4\pi\epsilon_0 r_{ab}} \quad (7)$$

where the two terms in the numerator, M_n^{0i} and M_m^{0j} are the three dimensional charge distributions (transition densities) associated with the ground and electronic excited states i and j of molecules n and m , respectively, with the separation between the elements a and b equal to r_{ab} . The V^{Coul} corresponds to the electrostatic repulsion energy between the two charge distributions M_n^{0i} and M_m^{0j} of isolated chromophores. The calculations of the Coulombic couplings using the three dimensional charge distribution takes into account the size and the spatial extent of the transition density and is valid at all molecular separations as opposed to the *ideal dipole approximation* (IDA). In the latter only the dipole moment of the transition density is considered for calculations of the coupling terms which makes the computations of the off-diagonal elements much more efficient. However, this approximation breaks down at the small donor-acceptor separations for which the spatial extent of the transition density becomes important.

To account for the dynamics of the DNA chain itself, we performed a series of molecular simulations of the 12 base pair duplex DNA (AT) (Figure 2) with about 12,000 water molecules and counter ions. [60] Once the system was minimized and equilibrated in the NVE ensemble at 300K, we integrated the dynamics for an additional 80 ps, sampling the DNA configuration every 10 fs. Even though we are dealing with a relatively small strand, it remains too large for an accurate evaluation of its electronic structure. Consequently, we make the approximation that the excited states of the molecule itself can be written as a linear combination of excited states localized on the instantaneous positions of each base along the chain. Furthermore, given the computational cost associated with evaluating the excited states of even a small molecule, it is prohibitive to perform such calculations

for each base at each time-step. Our approach, then, is to perform an accurate evaluation of the local transition densities based upon the geometries of the isolated DNA bases, then map these densities onto the instantaneous positions of the bases from the molecular dynamics simulations (Figure 2). From this, we can evaluate the exciton-exciton coupling (Eq. 7) in which M_n^{0i} and M_m^{0j} are the transition densities about the instantaneous positions of bases n and m .

2. Excited states of individual bases

The geometries of the DNA bases, adenine, guanine, cytosine, and thymine in their most common tautomeric forms were optimized at the MP2/TZVP level of theory in chloroform using Gaussian03 suite of programs.[31] The optimized geometries were subsequently used to calculate the singlet excitation energies in gas phase at the TD-DFT level using PBE0 functional and TZVP basis set augmented with the diffusion functions on all atoms as implemented in ORCA.[32] Additionally, the excitation energies were also calculated for the standard nucleobase geometries obtained from the X3DNA.[33] In these calculations the deoxyribose and phosphate groups were replaced with hydrogens using the Chimera program.[34] Without further optimization of the structures, the excitation energies were calculated at the same level of theory as used before for the MP2 optimized structures. Fig. 3 shows both the transition density and direction of the transition dipole moment for each base as given by TDDFT after optimization at the MP2/TZVP level in a CHCl_3 . Transition moments were calculated using TDDFT with PBE0 functional and aug-TZVP basis set in vacuum. The calculated excitation energies are summarized in Table I.

The transition densities associated with the allowed

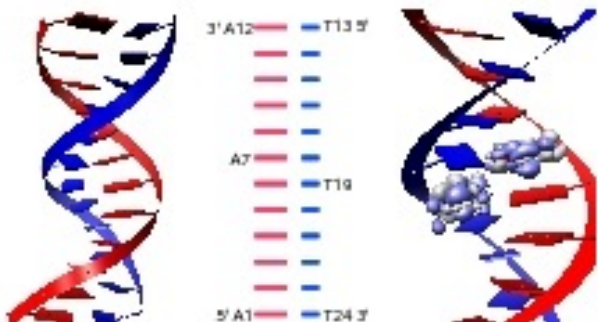


FIG. 2: Schematic structure of the $(\text{A})_{12}\cdot(\text{T})_{12}$ oligomer used in the MD simulations (left). The residue numbering is shown in the middle. The graphic on the right shows the three dimensional representations of densities corresponding to lowest energy $\pi\pi^*$ transitions of adenine and thymine superimposed with residues 7 and 19, respectively, of the $(\text{A})_{12}\cdot(\text{T})_{12}$ model.

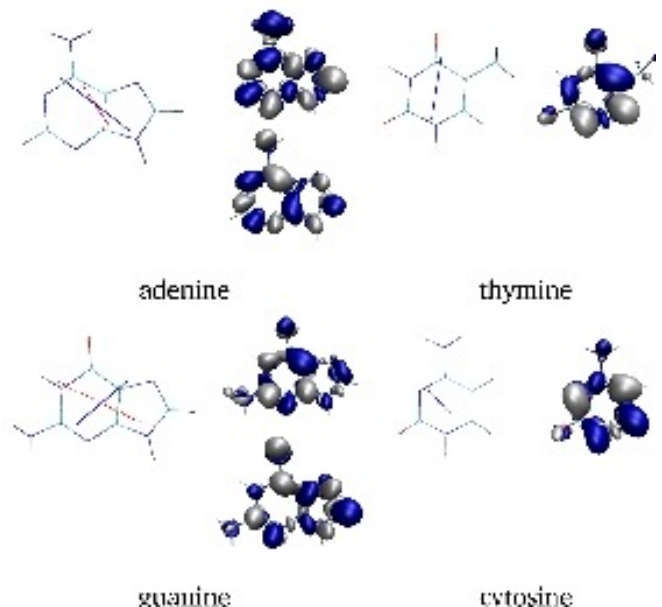


FIG. 3: The transition densities and transition moments in the nucleobases: adenine, thymine, guanine, and cytosine. For purines the solid and dotted lines indicate the direction of the transition dipoles associated with the first and second lowest energy $\pi\pi^*$ transitions, respectively.

$\pi\pi^*$ excitations of the individual nucleobases, defined by

$$M_{eg}(\mathbf{r}; s) = |\Psi_g\rangle\langle\Psi_e|dr \quad (8)$$

where e and g correspond to the excited and ground states of the chromophore, were calculated using ORCA program. The densities are written in form of a charge distribution over three-dimensional grid of points, such that the integrated charge vanishes, according to

$$M_{eg}(x, y, z) = V_\delta \int_z^{z+\delta_z} \int_y^{y+\delta_y} \int_x^{x+\delta_x} \Psi_g \Psi_e^* ds dx dy dz \quad (9)$$

where $V_\delta = \delta_x \delta_y \delta_z$ is the element volume and the δ_x , δ_y , δ_z are the steps along the coordinate axes. The grid size has to be a compromise between the accuracy and the speed. Denser grids render the calculations very taxing while too small grids introduce large errors in the calculated coupling elements. A satisfactory compromise was obtained for the cube files with 40 voxels along each axis (x , y , and z) which corresponds to total number of 64000 elements. In case of the single nucleobase the volume of a single element is than 0.03 \AA^3 . The changes in the magnitude of the coupling calculated for cubes with number of elements larger than 64000 was below 0.1 cm^{-1} . Owing to the finite size of the cube the integrated charge over space was not exactly zero. The residual charge for all the transition density cubes was below $0.01e$ and was compensated by adding equal amount of charge to each volume element to bring the integrated charge over the cube volume to zero.

TABLE I: Vertical singlet excitation energies (eV) followed by oscillator strength in parentheses of the lowest electronic transitions of the nucleobases calculated using TDDFT at PBE0/aug-TZVP level of theory and MRCI in vacuum for the standard geometries taken from 3DNA and optimized at MP2/TZVP level in chloroform. For the calculated excited state energies the transitions with a $\pi\pi^*$ character are indicated with a boldface.

	Method	Geometry	$S_0 \rightarrow S_1$	$S_0 \rightarrow S_2$	$S_0 \rightarrow S_3$	$S_0 \rightarrow S_4$	$S_0 \rightarrow S_5$
A	TDDFT	MP2	5.00 (0.002)	5.29 (0.230)	5.38 (0.069)	5.49 (0.009)	
		standard	5.17 (0.001)	5.44 (0.204)	5.46 (0.006)	5.52 (0.086)	
	MRCI	MP2	4.80 (0.168)	5.01 (0.003)	5.13 (0.446)	5.13 (0.004)	
	Exp. ^a		4.5–4.6	4.7–4.9	5.8–6.1		
G	TDDFT	MP2	4.84 (0.024)	5.07 (0.142)	5.22 (0.002)	5.24 (0.014)	5.42 (0.304)
		standard	4.58 (0.001)	5.04 (0.167)	5.08 (0.002)	5.25 (0.000)	5.41 (0.313)
	MRCI	MP2	3.68 (0.001)	4.74 (0.286)	5.18 (0.002)	5.21 (0.478)	5.57 (0.014)
	Exp. ^b		4.4–4.6	4.9–5.1	5.5	6.1–6.3	
T	TDDFT	MP2	4.74 (0.000)	5.22 (0.161)	5.66 (0.000)		
		standard	4.74 (0.000)	5.21 (0.156)	5.63 (0.000)		
	MRCI	MP2	4.63 (0.000)	5.35 (0.434)	5.74 (0.004)		
	Exp. ^c		4.6–4.7	5.6–6.1	6.4		
C	TDDFT	MP2	4.78 (0.049)	4.84 (0.000)	5.18 (0.002)		
		standard	4.70 (0.040)	4.77 (0.000)	5.07 (0.002)		
	MRCI	MP2	4.69 (0.151)	4.73 (0.002)	5.69 (0.007)		
	Exp. ^d		4.5–4.6	5.0–5.4	5.6–6.1		

Average experimental excitation energies from Refs. ^a [48, 49, 50] ^b [51, 52, 53, 54] ^c [50, 54, 55, 56] ^d [52, 55, 57, 58, 59]

The transition densities between the ground and excited states of the individual DNA bases were generated using TDDFT at the geometries of the bases optimized at MP2 level of theory, as described above. Before the actual calculation of the coupling elements could be carried out the transition densities and dipole moments obtained from *ab initio* calculations in an arbitrary coordinate system were transformed to the geometries of the bases in the studied DNA structures. This was carried out by defining the transformation superposing the plane defined by C6, N1, and N3 atoms of pyrimidine or C6, N1, and N9 atoms of purine bases in the arbitrary system with the plane defined by the corresponding three atoms of the base in the DNA structure. Subsequently, the transformation was applied to the three-dimensional grid holding the transition density and the dipole moments. The quality of the fit as measured by the root-mean squared deviation between the atom coordinates of the two overlapped structures was very good.

III. RESULTS AND DISCUSSION

A. Individual Nucleobases

The optimization of the standard nucleobase geometries [35] obtained from X3DNA [33] at the MP2 level has very small effect on their geometries. The only noticeable difference is the out-of-planarity of the NH₂ groups of adenine, guanine, and cytosine in the optimized geometries. This is in agreement with previous theoretical

studies of Shukla *et al.* ([36] and references therein) and experiment [37] where the amino groups of Ade, Gua, and Cyt were also found to be non-planar.. The root mean square deviations (RMSD) between the heavy atoms (excluding hydrogens) of the original and optimized structures is 0.045 Å for adenine (Ade), 0.040 for guanine (Gua), 0.017 Å for thymine (Thy), and 0.024 Å for cytosine (Cyt).

1. Excited-State Calculations

The MP2 optimized structures of the 9H-purines and 1H-pyrimidines were subsequently used to calculate the vertical excitation energies using time dependent density functional theory (TDDFT) at the PBE0/augTZVP level in gas phase. The results of the excited state calculations on Ade, Gua, Cyt, and Thy were also compared with the available experimental data and multireference configuration interaction (MRCI) calculations.

Adenine. The lowest TDDFT calculated vertical singlet excitation energies of adenine, 5.00, 5.29, and 5.38 eV (Table I) correspond to the $n\pi^*$ and two closely spaced $\pi\pi^*$ transitions, respectively. While this order is in agreement with other DFT calculations ([36]), *ab initio* calculations at CASPT2 level ([38]) has shown the lowest excited state, S_1 , to be a $\pi\pi^*$ state in agreement with the experiment. The UV-spectra of 9-methyladenine in stretched polymer poly(vinyl alcohol) films collected by Holmen ([39]) show two in-plane polarized transitions located at 4.55 and 4.81 eV. Contrary to the TDDFT

results the experimental data show the low-energy $\pi\pi^*$ transition to carry less oscillator strength. The higher level *ab initio* calculations performed at MRCI level also predict the lowest energy state to be the light absorbing $\pi\pi^*$ state, calculated at lower energy, 4.81 eV, compared with TDDFT results. The second $\pi\pi^*$ state is calculated at 5.07 eV. In accordance with the experiment and CASPT2 data the MRCI predicts the higher energy $\pi\pi^*$ transition to be more intense than the lower energy one. The most noticeable structural change, between the MP2 optimized and standard geometry of Ade is the pyramidalization of the amine N in the former. The calculated transition energies at the TDDFT level imposed by the pyramidalization show a blue shift in the range of 0.10–0.15 eV for the flat structure. However, the separation between the two $\pi\pi^*$ states and the character of the first excited state are not noticeably changed at this level of theory.

Guanine. For the structure with the planar geometry of the NH_2 group (standard geometry) the computed lowest excitation energy at 4.59 eV is classified as the $\pi\sigma^*$ transition. For this transition the configuration with the highest percentage weight, 99%, corresponds to $\text{HOMO} \rightarrow \text{LUMO}$, with the LUMO orbital being a σ^* localized at NH_2 group. The lowest energy $\pi\pi^*$ transitions for the flat structure are calculated at 5.04 and 5.41 eV. The pyramidalization of the NH_2 group in the MP2 optimized structure causes the lowest energy transition to acquire some π^* character. It is now calculated at higher energy 4.89 eV and defined by the configurations $\text{HOMO} \rightarrow \text{LUMO}$ (91%) and $\text{HOMO} \rightarrow \text{LUMO}+1$ (5%). At this geometry the LUMO orbital is a mixture of π^* and σ^* and the LUMO+1 is pure π^* . Similar mixing of π^* and σ^* character was reported by Leszczynski and coworkers, who assigned corresponding transition for the nonplanar structure to the weak $\pi\pi^*$ transition. In our calculations the two lowest energy $\pi\pi^*$ transitions are calculated at 5.07 and 5.42 eV and the transition at 4.89 eV is classified as $\pi\sigma^*$. For this assignment of the $\pi\pi^*$ transitions the difference in their calculated energies for the planar and pyramidal geometry of NH_2 group is very small, below 0.05 eV. A completely different situation was observed for the adenine, for which pyramidalization of the NH_2 group caused blue shift of the $\pi\pi^*$ transitions. The MRCI calculations yield the two lowest singlet vertical excitation energies at 4.24 and 4.34 eV which have $n\pi^*$ character. The lowest $\pi\pi^*$ transitions at this level of theory are calculated at 4.76 and 5.24 eV. The latter $\pi\pi^*$ transition has also larger calculated oscillator strength similarly to what was observed for adenine at this level of theory.

Thymine. The *ab initio* and TDDFT calculations predict the lowest energy $n\pi^*$ transition in vacuo for Thy in accordance with reported experimental data. The excitation energies calculated at the optimized and standard geometries of Thy are virtually the same for both the $n\pi^*$ and $\pi\pi^*$ transitions. In an aprotic solvent thymine has the $n\pi^*$ state as the lowest singlet excited state [40]. Present calculations at the TDDFT level, show dark $n\pi^*$

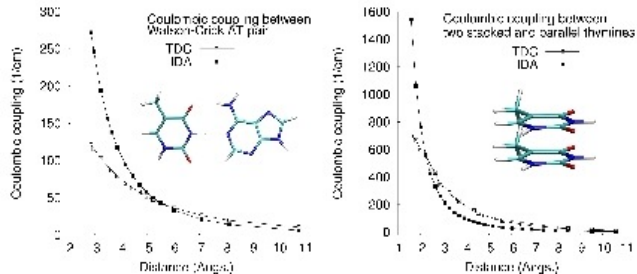


FIG. 4: Coulombic coupling between the lowest $\pi\pi^*$ transition moments of Watson-Crick AT base pair (left) and two stacked and parallel thymines (right) as a function of the distance between the two bases. The distance is measured between N1 and N3 atoms of A and T, respectively, for the AT pair (left) and between the centers of the masses of the two thymines (right).

singlet excited state calculated at 4.74 eV, approximately 0.5 below bright $\pi\pi^*$ state calculated at 5.22 eV. At the MRCI level the relative order of this two transitions is the same and the calculated energies 4.63 and 5.35 eV of the $n\pi^*$ and $\pi\pi^*$ transitions, respectively, are in good agreement with the corresponding TDDFT values.

Cytosine. The TDDFT computed vertical singlet excitation energies of cytosine, shown in (Table I), predict the $\pi\pi^*$ state to be the lowest energy transition calculated at 4.78 and 4.70 eV for MP2 and standard geometries, respectively. The non-planarity of the NH_2 has only small effect on the energy of the $\pi\pi^*$ transition inducing a red shift with a magnitude below 0.1 eV. The MRCI calculations predicts the same order of the two lowest transitions, with $\pi\pi^*$ below $n\pi^*$ and their energies within 0.1 eV of the corresponding TDDFT values (Table I).

B. Coulombic Coupling

The values of the Coulombic couplings between the lowest energy $\pi\pi^*$ transitions of the adenine and thymine and two π -stacked thymines as a function of distance between the bases (Fig. 4) were calculated using the TDC and IDA methods. For the calculations the transition densities and dipoles were those obtained from the TDDFT calculations on the MP2 optimized geometry of the bases. The comparison of the coupling elements obtained with the two methods, IDA and TDC, (Fig. 4) shows a good agreement at a separation between the bases larger than 5 and 6 Å for the AT pair and two stacked thyminess, respectively. At a shorter separations, in the range of 3–4 Å, which is typical for DNA structures, the agreement between IDA and TDC is very poor with the differences between calculated couplings larger than 100% in case of AT pair. The aforementioned good agreement between IDA and TDC at a larger and poor agreement at shorter separations between nucleobases indicate that the shape and spatial extent of transition den-

sity (Fig. 4) become important and cannot be neglected at distances between the bases typical for double helices DNA. The agreement between the two methods becomes very good in the limit of very large separation, ($> 8 \text{ \AA}$).

In order to compare the performance of the IDA and TDC method we calculated the coulombic couplings between the lowest $\pi\pi^*$ transitions of adenine and thymine bases for the interstrand Watson-Crick, intrastrand π -stacked, and diagonal arrangement (Fig. 1) of the base pairs for the $(A)_{10} \cdot (T)_{10}$ oligomer in the idealized B-DNA geometry (Table ??) generated using the 3DNA program[33] using the IDA and TDC approximations. The corresponding band-structure as given by Eq. 6 is shown in Fig. 5.

For the stacking and pairing distances corresponding to the idealized B-DNA geometry the coupling elements calculated with the IDA approximation result with several-fold larger absolute values compared with the corresponding values calculated using the TDC method. The largest differences between the two methods are obtained for the couplings between the π -stacked adenines. For the idealized B-DNA geometry the coupling between two adenines located on the same strand calculated using IDA, 872 cm^{-1} , is more than 5-fold larger compared with the value obtained using TDC 161 cm^{-1} . The differences in the calculated couplings using the same two methods for two stacked thymines are much smaller. For this base pair the Coulombic coupling calculated using IDA is equal to approximately 230 cm^{-1} , more than twice the value of 101 cm^{-1} obtained with TDC. The absolute values of the coupling elements between the second nearest neighbors located on the same strand are much smaller. At the IDA level of approximation the coupling between

the two adenines is only 57 cm^{-1} compared with 9 cm^{-1} calculated for the same base pairs using transition density cubes. The coupling between the two thymine bases on the same strand is even smaller – approximately 3 and 1 cm^{-1} for IDA and TDC methods, respectively.

The values of the calculated coupling elements give hint on the relative exciton delocalization along the thymine and adenine strands of the $(A)_{10} \cdot (T)_{10}$ oligomer. The band structure in Fig. 5 shows that the mobility of the exciton along the thymine strand is low with both methods, IDA and TDC, giving reasonable close results. The exciton mobility along the adenine strand, to the contrary, is quite different for the two methods. IDA, in this case, predicts more delocalized exciton states compared to TDC, which reflects larger magnitudes of the couplings calculated with the former method.

The magnitudes of the couplings between bases located on different strands (Table ??), which belong to the Watson-Crick base pairs, are also larger when calculated with IDA method. The average Coulombic coupling for the Watson-Crick AT base pair calculated using IDA is 230 cm^{-1} compared with 101 cm^{-1} obtained with TDC method. The magnitudes of the couplings between bases located on different strands, which does not belong to the Watson-Crick, the diagonal terms, are generally still quite large. Especially, the magnitude of the coupling between diagonal bases in the $5'$ -XY- $5'$ direction (r^+) is comparable with the coupling for the Watson-Crick base pairs (Table III). The values computed for the AT pair with the IDA and TDC methods are 163 and 109 cm^{-1} , respectively. These values are almost twice and four times larger compared with the coupling between the corresponding bases in the $3'$ direction (r^-) calculated with the IDA and TDC methods, respectively. From the results of Table ?? it is clear that the coupling elements are very sensitive with respect to the base sequence. The calculated Coulombic couplings for the π -stacked arrangement of the adenine bases are by far the largest. Using IDA method the calculated coupling elements are more than two-fold larger than the corresponding values calculated with IDA for almost all arrangements.

To investigate the effect of the structural fluctuations on the calculated couplings between the adenine and thymine basepairs we analyzed 4000 conformations of selected basepairs from the 80 ps molecular dynamics trajectories of the $(A)_{12} \cdot (T)_{12}$. The extracted 4000 snapshots span the whole 80 ps simulations with each snapshot taken every 20 fs. In Table III) the average values of the couplings calculated using IDA and TDC methods for selected pairs of the $(A)_{12} \cdot (T)_{12}$ oligomer are listed. The comparison of these values with corresponding couplings calculated for basepairs in their idealized B-DNA geometry (Table ??) shows some very interesting points. Comparing the maximum and minimum values of the coupling elements in Table III it can be seen that the magnitude of the couplings is very sensitive to the structural fluctuations observed in the MD simulations. The absolute value of the coupling can differ by as much as 1000 cm^{-1} for

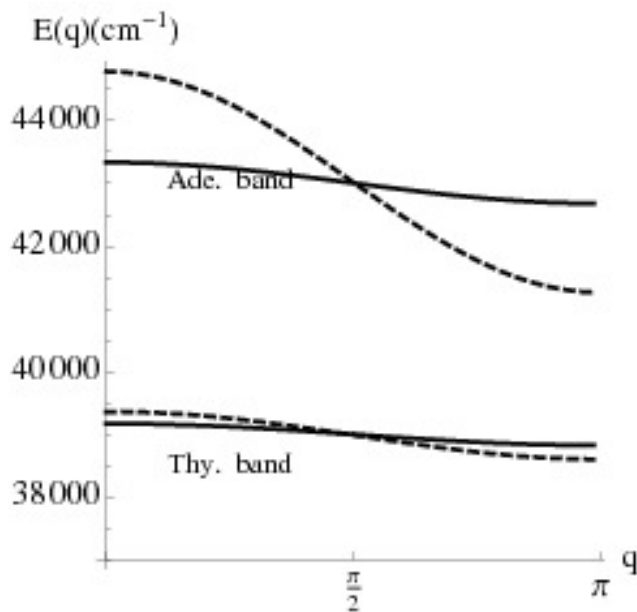


FIG. 5: Band structure for AT B-DNA. Dashed curves: IDA, Solid: TDC.

TABLE II: Average values of the Coulombic couplings (cm^{-1}) between the Adenine and Thymine bases of the $(A)_{10} \cdot (T)_{10}$ oligomer in the idealized BDNA geometry. The reported values are the averages for all corresponding base pairs with their standard deviations in parentheses. The h_n , t_n , and r_n^\pm correspond to coupling terms in Eq.5 and Eq.6.

	base 1	base 2	IDA	TDC
Watson-Crick Base Pairs				
h	A	T	229.5 (0.1)	100.8 (0.04)
π -stacked bases: nearest neighbors:				
t_A	A	A	871.7 (0.4)	160.7 (0.2)
t_T	T	T	201.4 (0.1)	90.2 (0.03)
π -stacked bases: 2nd nearest neighbors				
	A	A	57.4 (0.1)	8.7 (0.02)
	T	T	3.1 (0.005)	1.4 (0.002)
interchain diagonal cross terms				
r^+	A	T	163.4 (0.03)	109.1 (0.01)
r^-	T	A	90.7 (0.02)	25.2 (0.01)

π -stacked nucleobases. Other arrangements of the bases exhibit much smaller fluctuations of the couplings in the range of 300 cm^{-1} for Watson-Crick basepairs and still less for cross terms between bases on opposite strands and second nearest neighbors located on the same strand (Table III). The fluctuations of the couplings observed for the intrastrand nearest neighbors show also more complex pattern compared to these for Watson-Crick basepairs. An example is given by the couplings calculated with TDC method for the A9-A10 step (data not shown) of $(A)_{12} \cdot (T)_{12}$ oligomer. For this base pair the relatively larger and slower fluctuations on approximately 20 ps time scale are superimposed on the rapid fluctuations. Similar slower fluctuations are observed for other π -stacked adenines but not Watson-Crick pairs. For both π -stacked adenines and thymines the Coulombic coupling seems to also depend on the location of a given pair along the chain. As can be inferred from data in (Table III) the base pairs closer to the 3' end, A9-A10 and T21-T22 show larger average values of the couplings compared with the corresponding values calculated for the base pairs closer to the 5' end.

In spite of the large fluctuations of the couplings the values averaged over 4000 conformations are in good agreement with the corresponding couplings calculated for basepairs in standard B-DNA geometry. The best agreement is observed for the Watson-Crick base pairs while somewhat worse is seen for the π -stacked thymines. Interestingly, the average magnitudes of couplings for diagonal base pairs in the 5' and 3' directions are very similar when calculated using IDA method. The average couplings of the A8-T16 and A9-T17 base pairs calculated with this method for the 4000 conformations from the MD simulations are equal to 129 and 122 cm^{-1} , respectively (Table III). The transition density cubes calculated couplings, however still show sensitivity the direction with the average coupling in the 5' direction for A8-T16, 77 cm^{-1} , compared to only 33 cm^{-1} in 3'

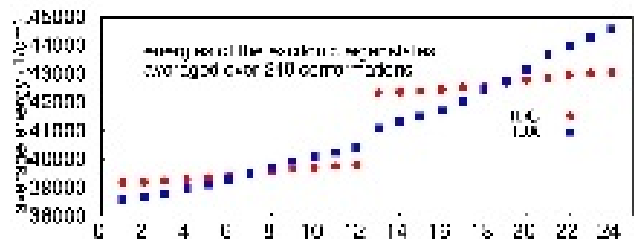


FIG. 6: Eigenstate energy of $(A)_{12}(T)_{12}$ averaged over 240 conformations from MD simulations obtained using TDC (filled circles) and IDA (filled squares).

direction for A9-T17.

C. Exciton states

In this section we compare the properties of the excited states of the double-stranded DNA model $(A)_{12} \cdot (T)_{12}$ calculated in the framework of the exciton theory where the off-diagonal elements of the exciton matrix were calculated using the ideal dipole approximation (IDA) and transition density cubes (TDC). The transition energies, oscillator strength, and the localization of the excited states were determined by diagonalization of the exciton matrix with the transition energies of the individual bases (diagonal terms) obtained from TDDFT calculations using standard geometries of the nucleobases while the coupling elements (off-diagonal terms) were determined using either IDA or TDC method. All properties were averaged over an ensemble of 240 conformations extracted from the MD simulations.

Fig. 6 shows the average values of the energies of the 24 eigenstates of the $(A)_{12} \cdot (T)_{12}$ obtained with the couplings calculated using TDC and IDA method. Using the former method for calculations of the coupling elements

TABLE III: Average Coulombic coupling \bar{V}_{ij} (in cm^{-1}) between selected bases of $(A)_{12} \cdot (T)_{12}$. The values are averaged over 4000 snapshots from an 80 ps MD simulation of DNA in water. σ is the r.m.s. deviation about the mean. Max. and Min. refer to the maximum and minimum value of the coupling over the entire simulation.

	base 1	base 2	\bar{V}_{ij}	σ	Max	Min
Interchain: Watson-Crick Base pairs						
IDA						
	A9	T16	235.7	29.9	325.8	105.2
	A4	T21	237.9	31.3	347.7	100.7
	A7	T18	235.8	33.3	363.0	112.0
TDC						
	A9	T16	109.3	11.7	151.6	71.4
	A4	T21	101.7	12.8	146.7	51.1
	A7	T18	99.7	15.3	146.3	39.3
Intrachain: nearest neighbor						
IDA						
	A3	A4	769.3	163.5	1338.4	322.0
	A6	A7	858.1	183.9	1378.9	284.2
	A9	A10	935.9	153.6	1396.6	434.1
	T21	T22	473.3	153.7	1007.4	18.6
	T18	T19	435.8	136.7	1041.8	110.9
	T15	T16	315.4	145.1	874.0	210.4
TDC						
	A3	A4	175.4	47.1	330.7	50.0
	A6	A7	197.2	65.4	363.7	0.0
	A9	A10	196.8	43.9	339.5	48.3
	T21	T22	164.9	45.9	338.9	38.0
	T18	T19	159.8	36.5	301.8	0.0
	T15	T16	124.2	39.7	277.3	17.4
Intrachain: 2nd nearest neighbor						
IDA						
	A3	A5	62.8	14.2	104.8	12.3
	T20	T22	25.1	15.5	74.2	24.8
TDC						
	A3	A5	11.9	8.2	41.6	13.8
	T20	T22	9.7	6.7	30.2	12.2
Interchain; diagonal terms						
IDA						
	A8	T16	129.0	32.3	238.0	28.2
	A9	T17	121.8	38.8	247.0	1.9
TDC						
	A8	T16	77.0	17.2	150.0	0.0
	A9	T17	33.0	9.9	73.5	0.0

the energies of the lowest 12 eigenstates are clearly separated from those of the remaining twelve eigenstates. The energy change between the two border eigenstates, $\langle 12 \rangle$ and $\langle 13 \rangle$, amounts to almost 2500 cm^{-1} while the difference between the highest and the lowest energy eigenstates in each of the two sets is less than 1000 cm^{-1} . The variations in the energy of a given eigenstate do not exceed 150 cm^{-1} . The abrupt energy change between

the two sets of eigenstates diminishes significantly when the IDA method is employed for calculations of the dipolar couplings (Fig. 6). The difference between the average energies of the border eigenstates $\langle 12 \rangle$ and $\langle 13 \rangle$ is less than 700 cm^{-1} with variations in the energies of these two eigenstates equal to 420 and 350 cm^{-1} , respectively.

The spatial extent of the eigenstates was evaluated based on the inverse participation ratio (*IPR*) of a given

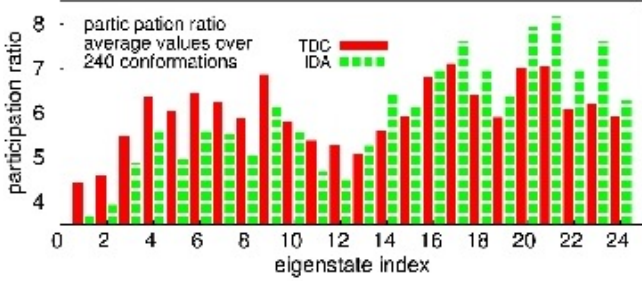


FIG. 7: Participation ratio of the 24 eigenstates of the $(A)_{12}(T)_{12}$. The values averaged over 240 conformations from MD simulations were calculated using TDC (solid lines) and IDA (dashed lines) methods.

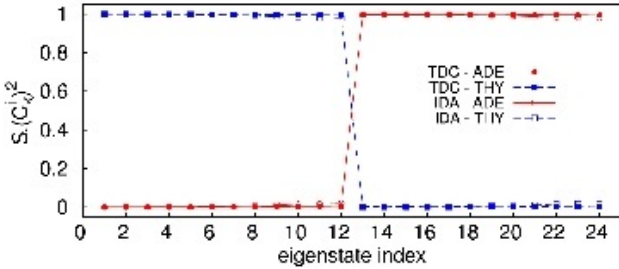


FIG. 8: Contribution of the S_2 states of thymine and adenine to the eigenstates of $(A)_{12}(T)_{12}$ oligomer.

eigenstate (Eq. 4), which indicates the number of coherently bound chromophores [41]. The plot in Fig. 7 shows the average IPR values for each of the 24 eigenstates calculated using TDC and IDA to obtain the coupling elements of the Hamiltonian matrix. The average values of the inverse participation ratios for $(A)_{12}(T)_{12}$ obtained with TDC are in the range between 4.5 and 7.1. The corresponding values obtained using TDC method are slightly smaller for the first 12 eigenstates and slightly larger for the remaining 12 eigenstates and are in the range between 3.7 and 8.2. In both cases the IPR values are much larger than one indicating delocalization of the excitation over several bases. Markovitsi *et al.* [4, 13, 14] showed that for the columnar aggregates of n identical chromophores, the maximum values of the normalized inverse participation ratio $1/nL_k$ is equal to 0.7. Therefore, in case of the $(A)_{12} \cdot (T)_{12}$ oligomer a completely delocalized eigenstate over one strand of the double helix would have a participation ratio equal to 8.4. Contrary to what Bouvier reported for the $(A)_{20} \cdot (T)_{20}$ and $(dAdT)_{10} \cdot (dAdT)_{10}$ oligomers, we found the participation ratios for all the eigenstates to be lower than 8.4. Therefore, a delocalization of the eigenstates over only adenosine or thymine chromophores but not both is expected. As can be seen from the contribution of the S_2 transitions of adenine and thymine to the eigenstates of the $(A)_{12} \cdot (T)_{12}$ (Fig. 8) the lower energy eigenstates are

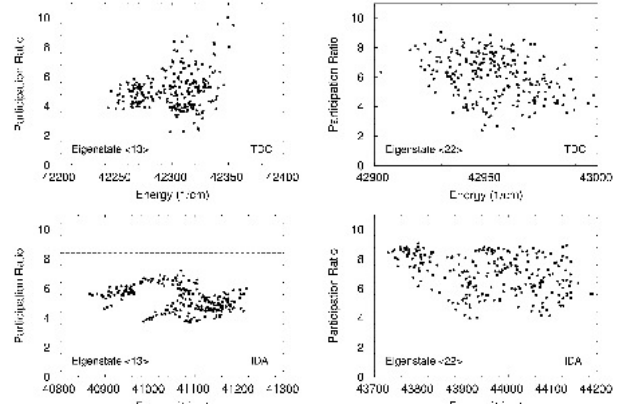


FIG. 9: Plot of the participation ratio of the eigenstate numbers $\langle 13 \rangle$ and $\langle 22 \rangle$ as a function of energy determined for 240 conformations of $(A)_{12}(T)_{12}$.

localized almost completely on the S_2 transition on the thymine, while the higher energy eigenstates are localized on the S_2 transition of adenosine.

The inverse participation ratios of the eigenstates $\langle 13 \rangle$ and $\langle 22 \rangle$ as a function of energy are plotted in Figure 9. The IPR values for these two eigenstates of $(A)_{12}(T)_{12}$ calculated for 240 conformations taken from the MD simulations show large fluctuations in the range of 2 – 10. Despite the wide range of calculated IPR values, as can be seen from the plots in Figure 9, the higher energy eigenstate, $\langle 22 \rangle$, on average shows larger delocalization compared with the lower energy eigenstate, $\langle 13 \rangle$, whether the IDA or TDC method was used to calculate coupling elements. However, only for a handful conformations the value of IPR exceeds the theoretical value of 8.4 (indicated by a dashed line in Figure 9) corresponding to the completely delocalized exciton over one strand of the $(A)_{12}(T)_{12}$. This indicates that both eigenstates $\langle 13 \rangle$ and $\langle 22 \rangle$ which are localized on the transition associated with adenine remains localized on only one strand of the $(A)_{12}(T)_{12}$ composed of adenine nucleobases.

The average values of the oscillator strengths versus the average energies of the eigenstates for 240 conformations from MD simulation are plotted in Figure 10. The total oscillator strength is distributed over a small number of eigenstates clustered in two bands. The first one comprise eigenstates $\langle 9 \rangle$ to $\langle 12 \rangle$ localized on thymine strand, and the second eigenstates $\langle 21 \rangle$ to $\langle 24 \rangle$ on adenine strand. The corresponding energies are around 39700 and 43000 cm^{-1} for the off-diagonal couplings obtained using TDC and 40100 and 44000 cm^{-1} for off-diagonal terms calculated with IDA. These “bright” states correspond to the higher energy eigenstates built on the thymine and adenosine monomer transitions (Figure 10), while their “dark” counterparts, carrying negligible oscillator strength, correspond to eigenstates with lower energies. The largest oscillator strengths are car-

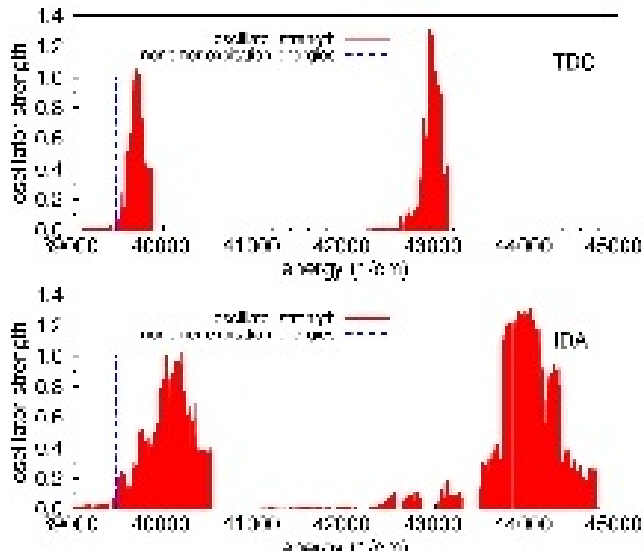


FIG. 10: Oscillator strength calculated for 24 eigenstates of the $(A)_{12}(T)_{12}$. The off-diagonal elements of the exciton matrix were calculated using the TDC (top) and IDA (bottom) methods. The values were averaged over 240 conformations extracted from the MD simulations.

ried by the eigenstates $\langle 10 \rangle$ and $\langle 22 \rangle$ and in both cases (IDA and TDA) the energies of these eigenstates are blue shifted with respect to transition energies of the individual bases. The magnitude of the shift approximately 1000 cm^{-1} and less than 500 cm^{-1} for IDA and TDC, respectively, reflects the differences in the couplings obtained with these two methods.

IV. CONCLUSIONS AND SUMMARY

We have investigated the properties of the excited states of $(A)_{12}(T)_{12}$ double helix calculated in the framework of the exciton theory. In our approach we combined the quantum mechanical calculations with the molecular dynamics simulations. The TDDFT calculations were employed to calculate the energies of the singlet excited states of the individual nucleobases. The transition moments and densities of the $S_0 \rightarrow S_2$ transitions of adenine and thymine which correspond to the lowest energy $\pi\pi^*$ transitions for these two bases were used to calculate the off-diagonal elements of the exciton matrix. The effect of the conformational changes were incorporated by averaging the calculated spectral properties of the double-stranded $(A)_{12}(T)_{12}$ over large number of the conformations extracted from the molecular dynamics simulations.

The Coulombic couplings calculated using the IDA and TDC methods show a large deviations for the distances between chromophores typical for the DNA double he-

lices. The magnitude of the couplings calculated with IDA being always larger than the corresponding values obtained with TDC. The agreement between the two methods is satisfactory only for the separations between the chromophores larger than 5 \AA . The largest difference between these two methods is observed for the π -stacked adenines in the standard B-DNA geometry for which the coupling calculated with IDA is over five times larger than the corresponding values calculated using TDC. The effect of the structural fluctuations on the calculated coupling elements is also very significant for both methods the values of the calculated coupling can change by an order of magnitude for different conformations of a given basepair. The difference between the smallest and largest coupling between the stacked adenines calculated using IDA for a given base pair can be as large as 1000 cm^{-1} , smaller but still significant difference in the range of 300 cm^{-1} was calculated using TDC.

The properties of the excited states of the $(A)_{12}(T)_{12}$ calculated in the framework of the exciton theory are affected to a different extent when the off-diagonal elements of the exciton matrix calculated using IDA and TDC methods. The eigenstates which carry the largest the oscillator strength, $\langle 10 \rangle$ and $\langle 22 \rangle$, are slightly blue-shifted with respect to the transition energies of single nucleobases (Figure 10). The larger shift, approximately 1000 cm^{-1} , is observed for the exciton states obtained with the off-diagonal elements of the exciton matrix calculated using the IDA approximation, compared to less than 500 cm^{-1} obtained with the dipolar coupling calculated using TDC method. However, the delocalization properties of these eigenstates is similar for both IDA and TDC couplings. The *IPR* values of the “bright” eigenstate $\langle 10 \rangle$ calculated with both IDA and TDC couplings are 5.5 and 6.0, respectively, while the corresponding *IPR* values of eigenstate $\langle 22 \rangle$ equal to 7.1 and 6.1 indicate only slightly large delocalization. Accordingly, comparing the *IPRs* obtained with TDC couplings the initial population of the bright eigenstates $\langle 10 \rangle$ and $\langle 22 \rangle$ by UV absorption will create exciton states which are delocalized over roughly 6 thymine and adenine bases, respectively. Upon relaxation the exciton states become more localized (Figures 9 and 7) as indicated by lower *IPR* values of the border eigenstates $\langle 1 \rangle$ and $\langle 13 \rangle$.

Acknowledgments

This work was funded in part by grants from the National Science Foundation and the Robert Welch Foundation. We are also grateful to Dr. Gillian C. Lynch and Prof. B. Montgomery Pettitt for providing us with the MD simulation data. We thank Dr. Stephen Bradforth for stimulating discussion motivating this work.

- [1] S. O. Kelley and J. K. Barton, *Science* **283**, 375 (1999), URL <http://www.sciencemag.org/cgi/content/abstract/283/5400/375>.
- [2] C. E. Crespo-Hernandez, B. Cohen, and B. Kohler, *Nature* **436**, 1141 (2005), URL <http://www.nature.com/doi/10.1038/nature03933>.
- [3] D. Markovitsi, D. Onidas, T. Gustavsson, F. Talbot, and E. Lazzarotto, *J. Am. Chem. Soc.* **127**, 17130 (2005).
- [4] D. Markovitsi, F. Talbot, T. Gustavsson, D. Onidas, E. Lazzarotto, and S. Marguet, *Nature* **441**, E7 (2006), URL <http://www.nature.com/nature/journal/v441/n7094/pdf/nature04903.pdf>.
- [5] A. Besaratinia, T. W. Synold, H.-H. Chen, C. Chang, B. Xi, and A. Riggs, *Proc Natl Acad Sci U S A* **102**, 10058 (2005).
- [6] B. M. Sutherland, R. Oliver, C. O. Fuselier, and J. C. Sutherland, *Biochem.* **15**, 402 (1976).
- [7] P. R. Callis, *Chem. Phys. Lett.* **61**, 563 (1979).
- [8] R. P. Sinha and D.-P. Hädler, *Photochem. Photobiol. Sci.* **1**, 225 (2002), URL doi:10.1039/b201230h.
- [9] S. E. Freeman, H. Hacham, R. W. Gange, D. J. Maytum, J. C. Sutherland, and B. M. Sutherland, *Proc Natl Acad Sci U S A* **86**, 5605 (1989).
- [10] S. Mouret, C. Baudouin, M. Charveron, A. Favier, J. Cadet, and T. Douki, *Proc Natl Acad Sci U S A* **103**, 13765 (2006).
- [11] P. O. Löwdin, *Rev. Mod. Phys.* **35**, 724 (1963).
- [12] T. Schultz, E. Samoylova, W. Radloff, V. H. Ingolf, A. L. Sobolewski, and W. Domcke, *Science* **306**, 1765 (2004), URL <http://www.sciencemag.org/cgi/content/abstract/306/5702/1765>.
- [13] E. Emanuele, D. Markovitsi, P. Millie, and K. Zakrzewska, *ChemPhysChem* **6**, 1387 (2005).
- [14] E. Emanuele, K. Zakrzewska, D. Markovitsi, R. Lavery, and P. Millie, *Journal of Physical Chemistry B* **109**, 16109 (2005).
- [15] C. E. Crespo-Hernandez, B. Cohen, and B. Kohler, *Nature* **441**, E8 (2006), URL <http://www.nature.com/nature/journal/v441/n7094/pdf/nature04904.pdf>.
- [16] J.-M. Pecourt, J. Peon, and B. Kohler, *J. Am. Chem. Soc.* **123** (2001).
- [17] J.-M. Pecourt, J. Peon, and B. Kohler, *J. Am. Chem. Soc.* **122** (2000).
- [18] T. Gustavsson, A. Sharonov, and D. Markovitsi, *Chemical Physics Letters* **351**, 195 (2002).
- [19] J. Peon and A. H. Zewail, *Chemical Physics Letters* **348**, 255 (2001).
- [20] A. Douhal, S. K. Kim, and A. H. Zewail, *Nature* **378**, 260 (1995), URL <http://www.nature.com/nature/journal/v378/n6554/abs/378260a0.html>.
- [21] S. L. Shapiro, A. J. Campillo, V. H. Kollman, and W. B. Goad, *Optics Communications* **15**, 308 (1975).
- [22] S. Suhai, *International Journal of Quantum Chemistry, Quantum Biology Symposium* **11**, 223 (1984).
- [23] B. P. Krueger, G. D. Scholes, and G. R. Fleming, *J. Phys. Chem. B* **102**, 5378 (1998).
- [24] J. Frenkel, *Physical Review* **37**, 1276 (1931).
- [25] A. S. Davydov, *Theory of Molecular Excitons* (McGraw-Hill, 1971).
- [26] E. R. Bittner, *The Journal of Chemical Physics* **125**, 094909 (pages 12) (2006), URL <http://link.aip.org/link/?JCP/125/094909/1>.
- [27] M. Creutz and I. Horvath, *Nuclear Physics B (Proc. Supp.)* **34**, 583 (1994).
- [28] J. A. McCammon and S. C. Harvey, *Dynamics of proteins and nucleic acids* (Cambridge University Press, Cambridge, 1987), 2nd ed.
- [29] C. Clelia, M. Michel, P. Francois, T. Benjamin, D. Iliana, and E. Mohamed, *The Journal of Chemical Physics* **122**, 074316 (2005).
- [30] A. L. Sobolewski and W. Domcke, *European Physical Journal D: Atomic, Molecular and Optical Physics* **20**, 369 (2002).
- [31] M. J. Frisch, G. W. Trucks, H. B. Schlegel, G. E. Scuseria, M. A. Robb, J. R. Cheeseman, J. A. Montgomery, Jr., T. Vreven, K. N. Kudin, J. C. Burant, et al., *Gaussian 03, Revision C.02*, Gaussian, Inc., Wallingford, CT, 2004.
- [32] F. Neese, *Orca - an ab initio, density functional and semiempirical program package, version 2.5. university of bonn* (2006).
- [33] X.-J. Lu and W. K. Olson, *Nucleic Acids Research* **31**, 5108 (2003), URL <http://rutchem.rutgers.edu/~xiangjun/3DNA/index.html>.
- [34] E. Pettersen, T. Goddard, C. Huang, G. Couch, D. Greenblatt, E. Meng, and T. Ferrin, *J. Comput. Chem.* **25**, 1605 (2004), URL <http://www.cgl.ucsf.edu/chimera/docs/credits.html>.
- [35] L. Clowney, S. C. Jain, A. R. Srinivasan, J. Westbrook, W. K. Olson, and H. M. Berman, *Journal of the American Chemical Society* **118**, 509 (1996).
- [36] J. Leszczynski and M. Skuhla, *J. Comput. Chem* **25**, 768 (2004).
- [37] F. Dong and R. E. Miller, *Science* **298**, 1227 (2002).
- [38] M. P. Fulscher, L. Serrano-Andres, and B. O. Roos, *J. Am. Chem. Soc.* **119** (1997).
- [39] A. Holmen, A. Broo, B. Albinsson, and B. Norden, *J. Am. Chem. Soc.* **119**, 12240 (1997).
- [40] P. R. Callis, *Ann. Rev. Phys. Chem.* **34**, 329 (1983).
- [41] B. Bouvier, T. Gustavsson, D. Markovitsi, and P. Millie, *Chemical Physics* **275**, 75 (2002).
- [42] *Esp: Extended systems program, copyright university of houston*.
- [43] J. A. D. MacKerell, D. Bashford, M. Bellott, J. R. L. Dunbrack, J. D. Evanseck, M. J. Field, S. Fischer, J. Gao, H. Guo, S. Ha, et al., *Journal of Physical Chemistry B* **102**, 3586 (1998).
- [44] H. C. Andersen, *Journal Computational Physics* **52**, 24 (1983).
- [45] J.-P. Ryckaert, G. Ciccotti, and H. J. C. Berendsen, *Journal Computational Physics* **23**, 327 (1977).
- [46] S. W. D. Leeuw, J. W. Perram, and M. L. Klein, *Proc. R. Soc. Lond.* **A373**, 27 (1980).
- [47] W. C. Swope, H. C. Andersen, P. H. Berens, and K. R. Wilson, *Journal of Chemical Physics* **76**, 637 (1982).
- [48] L. B. Clark, G. G. Peschel, and I. Tinoco, *J. Phys. Chem.* **116**, 3615 (1965).
- [49] L. B. Clark, *J. Phys. Chem.* **94**, 2873 (1990).
- [50] W. Voelter, R. Records, E. Bunnenberg, and C. Djerassi, *J. Am. Chem. Soc.* **90**, 6163 (1968).
- [51] L. B. Clark, *J. Am. Chem. Soc.* **116**, 5265 (1994).
- [52] D. Voet, W. B. Gratzer, R. A. Cox, and P. Doty, *Biopolymers* **1**, 193 (1963).

- [53] L. B. Clark, *J. Am. Chem. Soc.* **99**, 3934 (1977).
- [54] T. Yamada and H. Fukutome, *Biopolymers* **6**, 43 (1968).
- [55] C. A. Sprecher and J. W. Curtis Johnson, *Biopolymers* **16**, 2243 (1977).
- [56] W. C. Brunner and M. F. Maestre, *Biopolymers* **14**, 555 (1975).
- [57] F. Zaloudek, J. S. Navros, and L. B. Clark, *J. Am. Chem. Soc.* **107**, 7344 (1985).
- [58] K. Raksanyi, I. Foldvary, and L. K. J. Fidy, *Biopolymers* **17**, 887 (1978).
- [59] D. W. Miles, M. J. Robins, R. K. Robins, M. W. Winkley, and H. Eyring, *J. Am. Chem. Soc.* **91**, 831 (1969).
- [60] Regarding the molecular dynamics simulations: the simulation was performed with the extended system (ESP) molecular dynamics program [42]. The system consisted

of a 12 base pair duplex DNA (AT) with 11,593 waters, 46 sodium ions, and 24 chloride ions in a cubic box of length 70.4 Å. The atomic interactions were defined by the CHARMM (version 27) force field [43]. The system was minimized and equilibrated in the NVE ensemble at 300K. The bonds were kept rigid using the Rattle [44] implementation of the Shake method [45] and the electrostatic interactions were evaluated using the Ewald sum technique [46]. The equations of motion were integrated using the Velocity Verlet algorithm [47] with a 2 femtosecond time step. The simulation was initially run for 15 nanoseconds. Next, the timestep was changed to 1 femtosecond and the snapshots saved every 10 steps.